journal

J. Am. Ceram. Soc., 95 [8] 2531–2536 (2012)
DOI: 10.1111/j.1551-2916.2012.05240.x

Defect Structure of Flash-Sintered Strontium Titanate

Aylin Karakuscu,[‡,†] Marco Cologna,[§] Dmitry Yarotski,[¶] Jonghan Won,[‡] John S. C. Francis,[§] Rishi Raj,[§] and Blas P. Uberuaga[‡]

[‡]Materials Science and Technology Division, MST-8, Los Alamos National Laboratory, Los Alamos, New Mexico 87545

[§]Department of Mechanical Engineering, University of Colorado at Boulder, Boulder, Colorado 80309-0427

[¶]Center for Integrated Nanotechnologies, CINT, Los Alamos National Laboratory, Los Alamos, New Mexico 87545

Flash sintering of strontium titanate ($SrTiO_3$) is studied at different applied fields to understand its effect on density and grain growth. In particular, the defect structure is investigated by optical and structural analysis. $SrTiO_3$ exhibited a trend in densification opposite that of ionically or electronically conductive ceramics: as the applied voltage decreased, the density increased. Abnormal grain growth in conventionally sintered $SrTiO_3$ is arrested by flash sintering. Interestingly, undoped $SrTiO_3$ behaved differently than undoped Al_2O_3, which did not exhibit any signs of flash sintering. Previous attempts at flash sintering could only be achieved in MgO-doped Al_2O_3. We believe that non-stoichiometric Ruddlesden-Popper phases in $SrTiO_3$, as indicated by ultrafast optical spectroscopy, X-ray diffraction, conductivity measurements, and transmission electron microscopy, assist flash sintering by increasing local conductivity through enhanced defect content.

I. Introduction

Electric current-assisted sintering or simply Field-Assisted Sintering Techniques (FAST) have advantages, compared to conventional methods, of reduced sintering time and temperature by adding an electric field to the standard controls of time, temperature, and pressure.[1] The most well-known example is spark plasma sintering (SPS), which uses electrical heating of graphite dies along with uniaxial pressure. This widely used sintering method has been demonstrated to give high density, small grain size, and clean grain boundaries with enhanced sintering rates.[2]

A novel electric current-assisted sintering method – flash sintering – is attracting attention because of superior time and temperature reduction without the need of high pressure unlike SPS. Flash sintering has been demonstrated to be an innovative sintering method for ionic conducting[3] and electronic conducting[4] ceramics. Recently, yttria-stabilized tetragonal zirconia and cobalt manganese oxide spinel were successfully sintered at 850°C and 325°C, respectively, in a few seconds under an applied DC electric field. To achieve dense compacts of these materials via conventional sintering requires temperatures greater than 1000°C for several hours. Similar to other FAST sintering methods, flash sintering has produced nanomaterials without any substantial grain growth compared to the original powder.[3] For the first time, we report on flash sintering of $SrTiO_3$, a complex, undoped insulator. This work demonstrates that flash sintering can be used to sinter a wide range of ceramic materials. Microstructural as well as optical characterization is performed to give insight into the defect structure formed during flash sintering.

II. Experimental Procedure

Strontium titanium oxide, $SrTiO_3$ powder (Alfa-Aesar, Ward Hill, MA) with 99.9% purity is used as received. The powder has a specific surface area of 20m²/g, with an average particle size of 0.15 μm and a density of 4.81 g/cm^3. It is mixed with 5 wt% polyvinyl alcohol (mw 49000; Fluka, Sigma Aldrich, Milawaukee, WI) in water to improve the green body strength. The amount of polymer is kept to a minimum to prevent contamination at the grain boundaries. Powder is uniaxially pressed into a dog bone shape with a relative green density of 50%. The process is explained in detail in a previous study.[5]

The binder is completely removed after pre-heat treatment at 500°C for 5 h with rate of 2°C/min. Sintering was performed in a vertical furnace by suspending the samples by two platinum wires in the furnace.[3] The voltage at the two electrodes was kept constant, while the furnace temperature was increased from RT to 1400°C with a heating rate of 10°C/min. Once the sample reached the "flash sintering" regime,[3] the heat treatment is stopped and the sample left in the furnace as it cools. This regime can be considered as the densification stage of the samples.[6] A conventionally sintered sample, sintered without any applied voltage (0 V), is prepared for comparison. It is sintered by one step sintering, using the same furnace and conditions at 1400°C for 1 h.

The dimensions of the suspended sample were recorded with a CCD camera through a silica window and a low pass filter (KG3 Shott), positioned in series before the camera.[7] The shrinkage strain is calculated as the true strain, $\varepsilon = \ln(l/l_0)$, where l is the time-dependent gage-length and l_0 is the initial gage length.

(1) Characterization

Field emission scanning electron microscopy (FE-SEM) and focused ion beam/high resolution scanning electron microscope (FIB-SEM) were used to examine the microstructure of the flash sintered and conventional sintered samples. Microstructural studies on $SrTiO_3$ samples were done at the University of Colorado, Boulder with a JSM-7401F FE-SEM (JEOL Ltd., Akishima, Tokyo, Japan) and Los Alamos National Laboratory by FEI Strata DB235 FIB-SEM; FEI Company, Eindhoven, the Netherlands. Electron backscatter diffraction (EBSD) was performed at 20 kV in an FEI XL30 SEM equipped with TSL/EDAX data acquisition software. The orientation data were analyzed using TSL/EDAX OIM^{TM} Analysis software. 0.2 μm step size scans of areas 20 μm× 20 μm were performed. Small area scans were

P. Davies—contributing editor

Manuscript No. 30280. Received September 06, 2011; approved April 02, 2012.
†Author to whom correspondence should be addressed. e-mail: aylin.karakuscu@ing.unitn.it

preferred due to charging of the sample. Several scans were run to cover a greater area and obtain results representative of the entire sample. The number of analyzed grains was larger than 1000 for each sample.

Transmission electron microscopy (FEI Tecnai F30 analytical TEM; FEI Company, Eindhoven, the Netherlands) was applied to study the microstructure. The images were recorded by a high-resolution charge-coupled device camera (Ultrascan 4000 4k x4k CCD camera; Gatan, Pleasanton, CA). X-ray Diffraction measurements were made on the Rigaku Ultima III diffractometer that uses a fine line sealed Cu tube to generate Kα (λ = 1.5406 Å) X-rays. The generator is a D/MAX Ultima series with a maximum power of 3 kW. The bulk densities (ρ) of the samples were measured by Archimedes' method.[8] The porosity of the samples was calculated from the bulk density, using a value of 5.13 g/cm^3 for fully dense $SrTiO_3$. Ultrafast optical spectroscopy measurements were performed in a pump-probe geometry and employ 50fs laser pulses generated by an amplified Ti:Sapphire system at 250 kHz (Coherent RegA9500; Coherent Inc., Santa Clara, CA). The pump pulses were centered at 266 nm (4.5 eV) while probe pulses were tuned to 520 nm (2.4 eV). The pump beam is modulated at 3 kHz by a mechanical chopper and a lock-in amplifier (Stanford Research Systems SR830, Sunnyvale, CA) was used to extract transient reflectivity changes from the probe signal. The pump beam fluence was kept at ~0.1 mJ/cm^2, while the probe beam fluence was fixed at ~0.1 μJ/cm^2. All measurements were performed at room temperature (T = 295 K). Finally, conductivity measurements were done in two-point contact mode on flash sintered and conventional sintered $SrTiO_3$. The conductivity of sintered specimens is measured in cyclically applied electrical fields of various amplitudes and details are given elsewhere.[5]

III. Results and Discussion

(1) Flash Sintering and Microstructural Changes

Sintering curves of the flash sintered $SrTiO_3$ at three different voltages are in Fig. 1. For an applied voltage of 1000 V/cm, flash sintering conditions are achieved at 740°C with the sintering occurring in just a few seconds. The sintering process is hindered due to the limitation of the maximum current, which is kept at 60 mA (max. power 120 W). The density of this sample (<70%) is found to be too low for additional study. To improve the density, the maximum current is kept the same while the voltage is decreased to 500 V/cm. Under these conditions, flash sintering occurs at 900°C with a final linear shrinkage of 27%. The decrease in voltage causes the sintering temperature to increase from 740°C to 900°C. Final grain size is examined by SEM in Fig. 2. It retains the starting 150 nm powder size, while the density increases to 76% of the theoretical density. This result demonstrates the reverse relationship between voltage and sintering temperature as well as the relationship between these variables and sintered density.

The sintering conditions are optimized—highest densities and smallest grain sizes—when the voltage is fixed to 150 V/cm and the maximum current is increased to 500 mA. Flash sintering conditions is achieved at around 1200°C with a significant grain growth, as shown in Fig. 3. The average grain size is around 1 μm while the density is greater than 95% of theoretical density. The estimated density based on the shrinkage is 4.75 g/cm^3, which agrees well with our measured density. The sintering rate at this voltage is lower than for the other sintering conditions examined. The sudden grain growth and lower sintering rates suggest that the sintering conditions tend to change from the flash sintering to the FAST sintering regime. Note that flash sintering describes an instantaneous sintering, whereas FAST sintering is a gradual increase in shrinkage rate.[3]

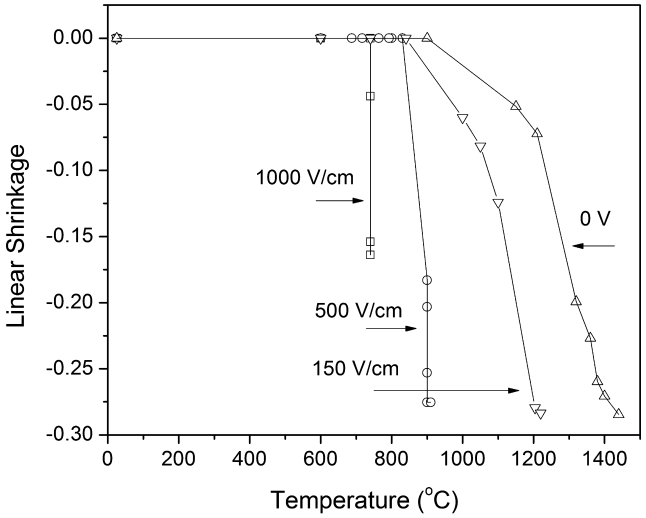

Fig. 1. Linear shrinkage with different applied electrical fields versus furnace temperature at constant heating rate of 10°C/min.

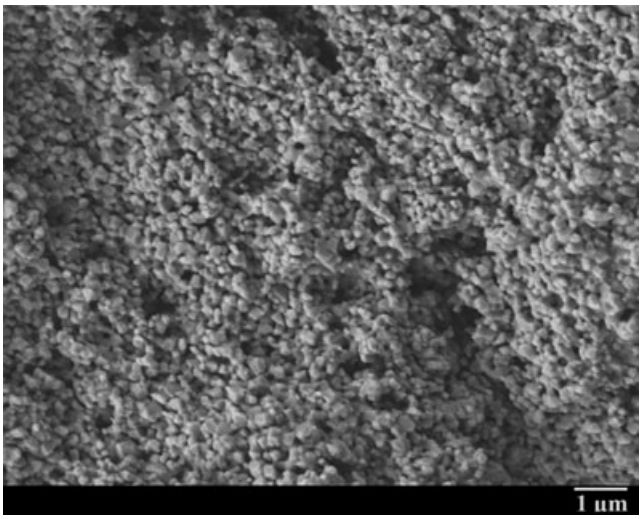

Fig. 2. SEM image of the flash sintered $SrTiO_3$ at 500 V/cm. Flash sintering occurred at 900°C.

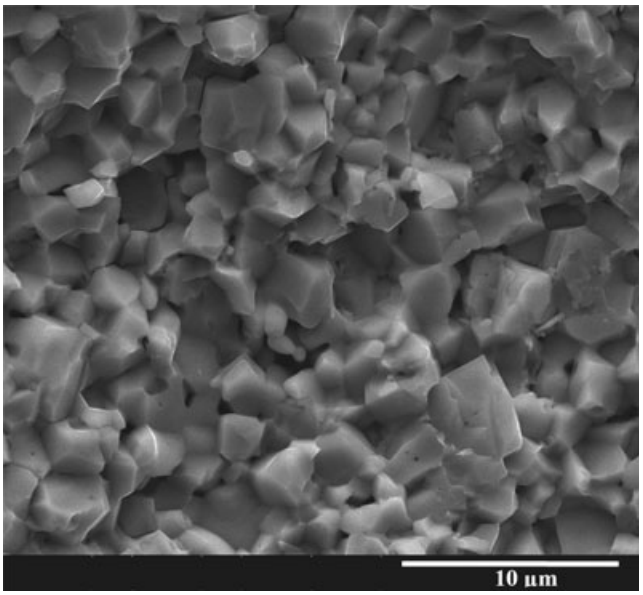

Fig. 3. SEM image of the flash sintered $SrTiO_3$ at 150 V/cm. Flash sintering occurred at around 1200°C.

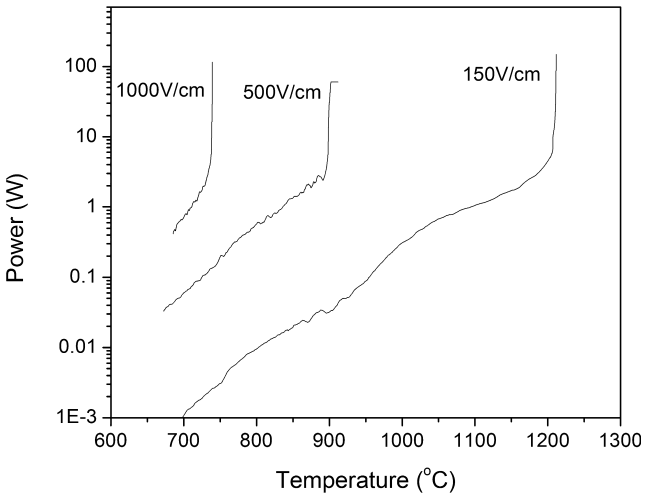

Fig. 4. Arrhenius plots for the power dissipation in $SrTiO_3$ samples at different values of the applied field.

Arrhenius plots of power-dissipation are reported in Fig. 4. A sudden power surge, characteristic of flash sintering, occurs above 5 W at 1000 and 500 V/cm. This critical power dissipation level is slightly higher at 150 V/cm, which confirms the transition from flash to FAST sintering. Finally, the power dissipation level observed here is the highest reported value among all previous studies, which is likely due to the relatively high resistivity of $SrTiO_3$; it is known that the field required for flash sintering decreases as conductivity increases.[3]

Conventional sintering is done at 1400°C for 1 h of soaking time to further insight into the flash sintering process. The average grain size for the conventionally sintered material is found to be 1.5 μm with a high grain size gradient across the sample (Fig. 5). The final density obtained is only 92% of theoretical density. Density and particle size change with respect to furnace temperature are shown in Fig. 6. The applied voltage is given as a dashed line to reveal its effect on the other parameters. Particle size remains constant until 900°C with 500 V/cm applied field and increases linearly afterward. Similar behavior is reported for spark plasma sintering where the grain size remains constant until a critical temperature is reached.[2] This critical temperature for $SrTiO_3$ should be higher than 900°C since grain size increased abruptly after this temperature. On the other hand, this temperature can be controlled and, most significantly, reduced by an applied voltage; higher voltages give lower sintering temperatures.

Electron backscatter diffraction is performed to explore the possible texture formation due to electrical field usage in flash sintering and to characterize the grain boundary structure of flash sintered and conventionally sintered $SrTiO_3$. Due to the non-conductive nature of $SrTiO_3$, several small area scans (about 20 μm × 20 μm) are done on carbon-coated samples (thickness of 30–50 nm) along the sample normal direction. Orientation image maps (OIMs) obtained on $SrTiO_3$ samples sintered at 150 and 0 V/cm (conventional sintering) are given in Figs. 7(a) and 8(a), respectively. Each of the image maps of these figures is then converted into a size histogram. The average grain size for flash sintered $SrTiO_3$ [Fig. 7(b)] is 0.9–1 μm, with a small outlying population (0.2% area fraction) of larger grains with sizes of 1.2–1.4 μm. Figure 8(b) shows a similar histogram for conventionally sintered $SrTiO_3$, but with wider grain size distribution (1.7–3 μm). With increasing sintering time and temperature, the fraction of large grains increases, as does their average size. The EBSD and FE-SEM results are evidence that flash sintering acts to stop abnormal grain growth, which is observed to a greater degree in conventionally sintered $SrTiO_3$.

In our previous work, we demonstrated that both the average grain size and density increase with increasing applied voltage in yttria-stabilized zirconia (YSZ), which is the

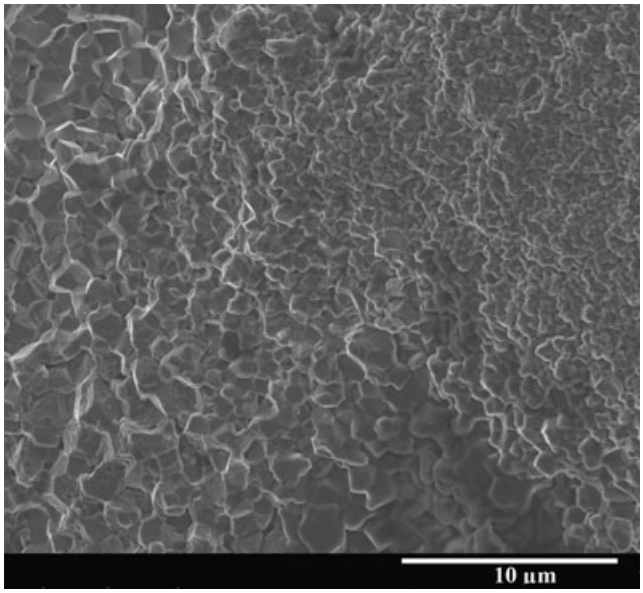

Fig. 5. SEM image of the conventionally sintered $SrTiO_3$ at 1400°C for 1 h.

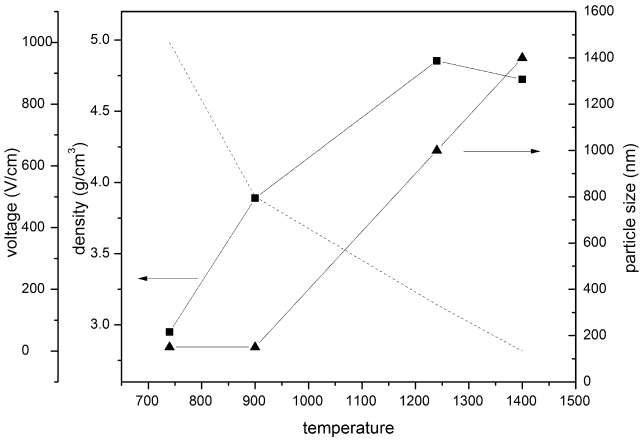

Fig. 6. Change in density (■) and particle size (▲) of the $SrTiO_3$ sample with respect to furnace temperature. Voltage (dashed line) is given to show the experimental conditions.

opposite trend observed here for $SrTiO_3$. This may suggest that the flash-sintering mechanism in non-conductive ceramics is different than in ionically or electronically conductive ceramics (YSZ, Co_2MnO_4, etc.). An additional decrease in voltage from 150 V/cm to 0 V does not improve the density but rather leads to a decrease in density. The density of conventionally sintered $SrTiO_3$ at 1400°C is 5% lower than the sample flash/FAST sintered at 1200°C. This shows that density can be improved and grain size refined at lower temperatures by flash sintering even in non-conductive ceramics.

(2) Defect Structure Analysis

Although it has been demonstrated that flash and FAST sintering methods (i.e., spark plasma sintering) have advantages over conventional sintering by decreasing temperature and time, the defect chemistry in these systems is not understood completely. Flash sintering, occurring in only a few seconds under an applied electrical field is a complex process, resulting in extra difficulties in understanding the resulting defect structure completely. The following section is an initial investigation into the defect structure of flash sintered $SrTiO_3$.

Optical characterization methods are very effective for analyzing defect states in the material, especially sensitive to even small numbers of defects. In this work, we used ultrafast

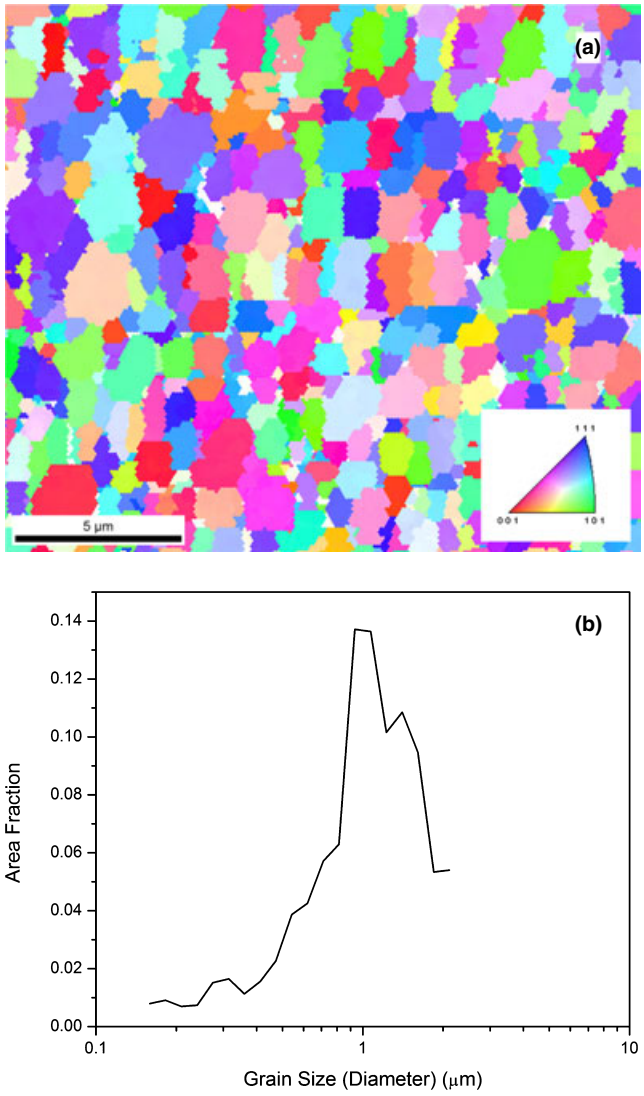

Fig. 7. (a) The [001] color-coded inverse pole figure map, generated with TSL/EDAX OIM^{TM}, shows the orientation and shape of the grains obtained on flash sintered $SrTiO_3$ polycrystalline at 150 V/cm. Grain orientations with respect to the sample normal are colored according to the standard stereographic triangle on the right. (b) The area fraction of grains with respect to average grain diameter is plotted for representative areas of the flash sintered $SrTiO_3$ at 150 V/cm.

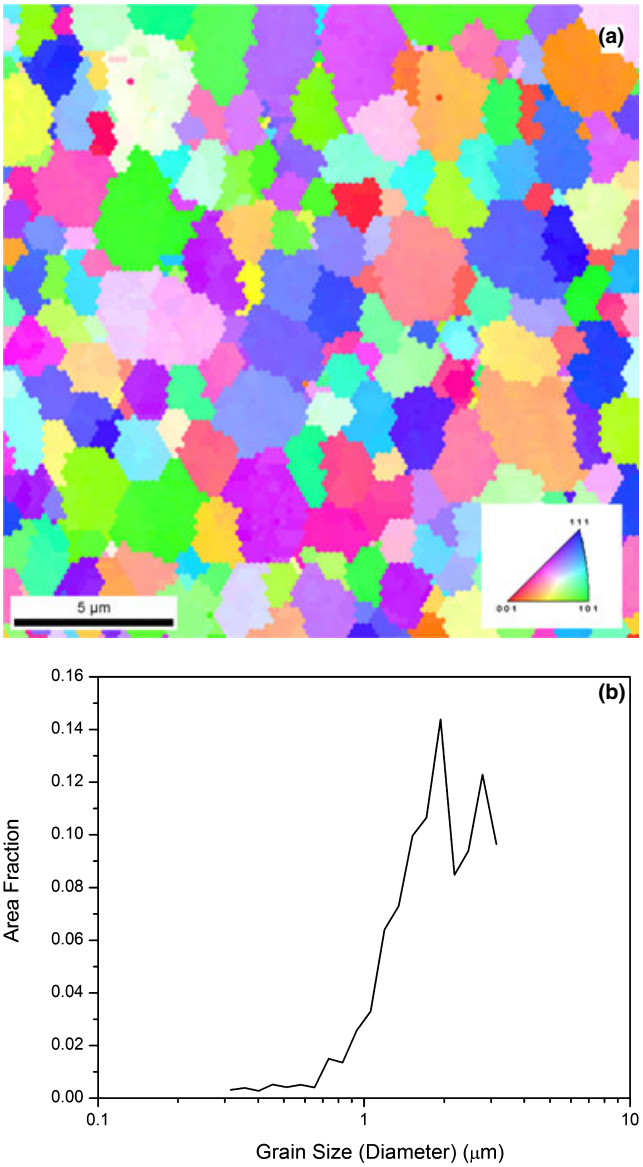

Fig. 8. (a) The [001] color-coded inverse pole figure map, generated with TSL/EDAX OIM^{TM}, shows the orientation and shape of the grains obtained on conventionally sintered $SrTiO_3$ (0 V). Grain orientations with respect to the sample normal are colored according to the standard stereographic triangle on the right. (b) The area fraction of grains with respect to average grain diameter is plotted for representative areas of the conventionally sintered $SrTiO_3$.

optical spectroscopy, which is very sensitive to defect states and changes in bonding structure, to study the defect states in $SrTiO_3$. Figure 9 shows the photoinduced reflectivity dynamics $\Delta R/R$ of conventionally sintered (0 V) and flash-sintered (150 V/cm) $SrTiO_3$ as a function of time delay between pump and probe pulses. The general feature of the dynamics observed in the different samples is the fast (~100 ps) relaxation of photo-induced changes back to the equilibrium value. This can be attributed to electron-phonon scattering with subsequent electron-hole recombination and lattice relaxation processes. In single-crystal $SrTiO_3$ (MTI corporation, Richmond, CA) electron-hole recombination is slow (>1000 ps). The difference between the sintered and the single crystal response suggests that this is a direct consequence of a finite residual defect concentration remaining due to sintering and/or distortions, which can also act as defects in terms of their effect on the reflectivity dynamics. These defects are charge traps or scattering centers, providing additional routes for charge-lattice relaxation in the crystal structure. The fact that the relaxation in both flash and conventionally sintered polycrystals occurs on almost the same timescale indicates that the photoinduced reflectivity dynamics of both samples is very similar. The difference in signal amplitudes, however, might be related to gradients in grain size that causes scattering.

There are three primary possibilities for the source of the enhanced electron-hole recombination: impurities, secondary phases, or point defects within the $SrTiO_3$ structure. The possibility of impurity content coming from the sintering process (specifically the binder) was investigated using particle induced X-ray emission (PIXE). No impurities are detected (<10 ppm) within the sample, ruling out the first possibility. Sintered samples as well as the starting powder, for comparison, were analyzed by XRD. All samples are cubic $SrTiO_3$ in the *Pm3m* structure with a small shift in Fig. 10(a), which is highlighted in Fig. 10(b), where the most intense (110) peak is shown. The peak for the starting powder, centered at 32.4°, shifts to higher 2θ values in both the sintered samples, indicating that the lattice parameter is becoming smaller upon sintering. The starting powder has lattice constant of $a = 3.905$ Å (JCPDS#73-0661) while the sintered samples have smaller lattice constants (around 3.89 Å),[9] an effect that

is slightly greater in the conventionally sintered sample than that in the flash sintered sample. These shifts are attributed to distortions in the structure due to sintering, which is consistent with the ultrafast optical spectroscopy results. Such distortions in the structure can be caused by defects (such as oxygen vacancies) or local non-stoichiometric phases, both of which can cause a radical difference in optical response of the material.

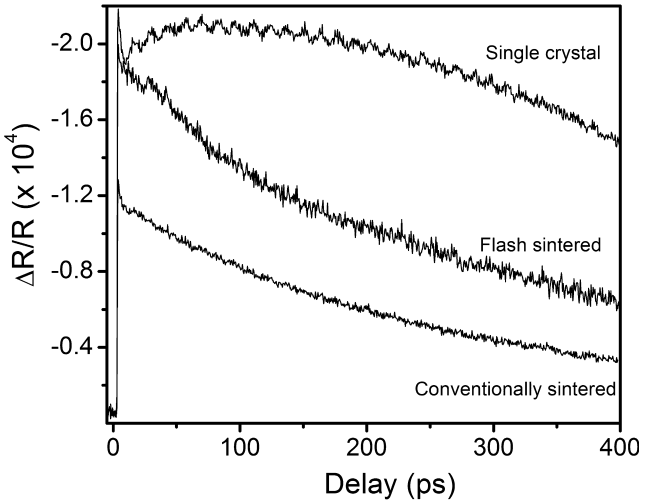

Fig. 9. The photoinduced reflectivity dynamics $\Delta R/R$ of conventionally and flash-sintered $SrTiO_3$ as a function of time delay between pump and probe pulses. Single crystal $SrTiO_3$ is also analyzed to compare polycrystalline samples with defect-free structure.

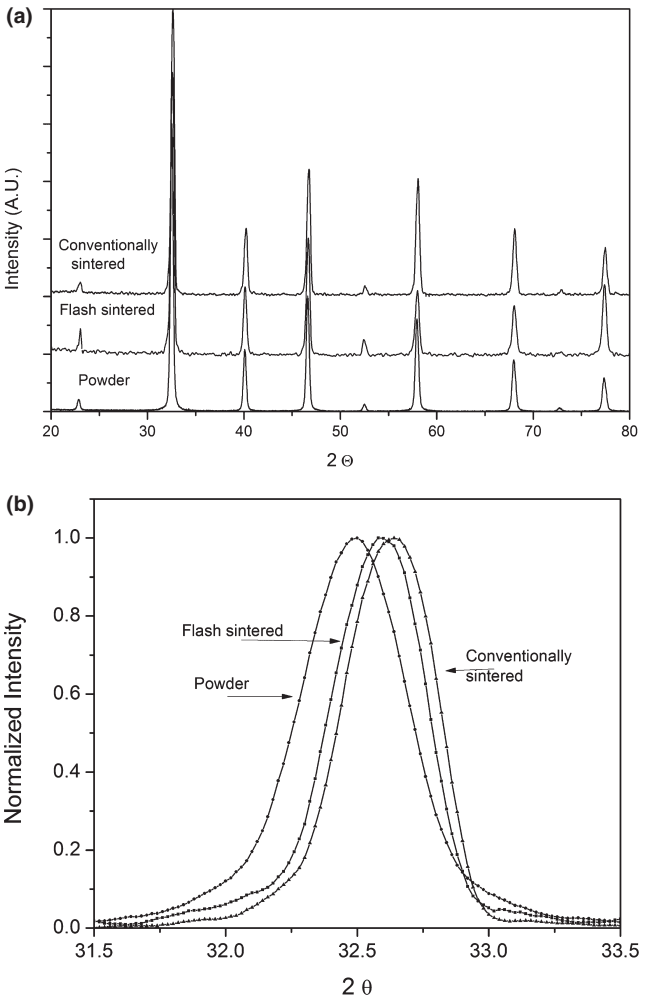

Fig. 10. (a) XRD spectra of flash sintered and conventionally sintered $SrTiO_3$. Starting powder is analyzed to reveal the structural differences during sintering process. (b) (110) peaks of all samples are given separately to demonstrate the peak shift toward high θ values.

The TEM analysis of the microstructure was performed to understand the type of defect structure which might be responsible for the peak shift in the XRD and the changes observed in the reflectivity dynamics. As for the XRD results, microstructure analyses by means of High Resolution Transmission Electron Microscopy (HRTEM) imaging and micro-beam electron diffraction patterns (MBEDP) indicated that sintered material has a stoichiometric $SrTiO_3$ cubic structure (*Pm-3m*). However, some of the grains have defect structures with irregularly spaced line features, as shown in the HRTEM image in Fig. 11. These defects are explained by local chemical deviations from stoichiometric $SrTiO_3$ and are referred to as Ruddlesden-Popper (RP) phases [SrO $(SrTiO_3)_n$ or $Sr_{n+1}Ti_nO_{3n+1}$].[10] They are introduced by the accommodation of long-range order lattice distortion and explained by self-healing of vacancy distortion by insertion of shear planes.[11–13] During sintering, structure can change significantly by reduction or oxidation at elevated temperatures. Structural distortions in stoichiometric SrTiO3 under an applied electric field have been reported and explained by the ordering of oxygen vacancies and electro-migration of SrO ion complexes.[14] Indeed, it has been reported that RP phases cause the existence of RP phases induce a shift to the right in the positions of XRD peaks as n gets smaller.[15–18] This is consistent with our XRD results. The initial powder is stoichiometric $SrTiO_3$ with $n = \infty$; as non-stoichiometric RP phases are formed in the material, the average value of n decreases.

Finally, conductivity measurements are shown in Fig. 12. The temperature dependence of the electrical conductivity (σ) of $SrTiO_3$ samples follows an Arrhenius law. The activation energy values for flash sintered and conventional sintered $SrTiO_3$ agree well with literature values for $SrTiO_3$.[19] On the other hand, both flash and conventional sintered $SrTiO_3$ exhibit higher absolute conductivities compared to the literature values. This difference in the conductivity is within the range of the experimental error but can also be

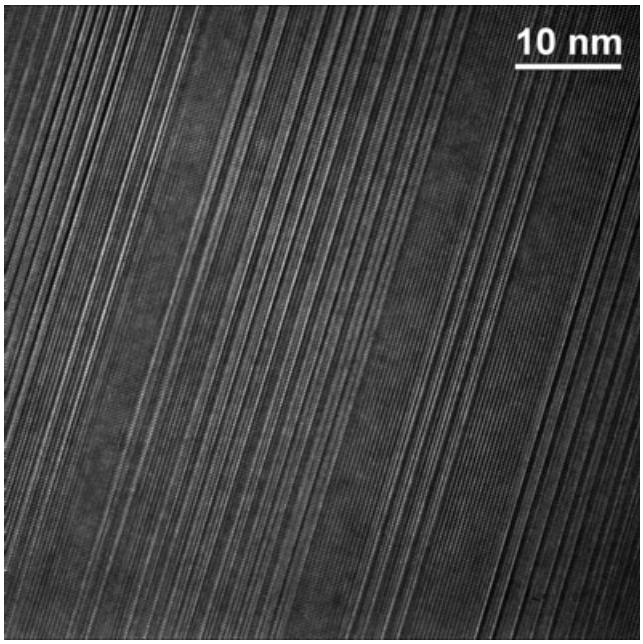

Fig. 11. TEM image of flash sintered $SrTiO_3$ at 150 V/cm. Some regions contain Ruddlesden-Popper phases, caused by long-range order lattice distortions.

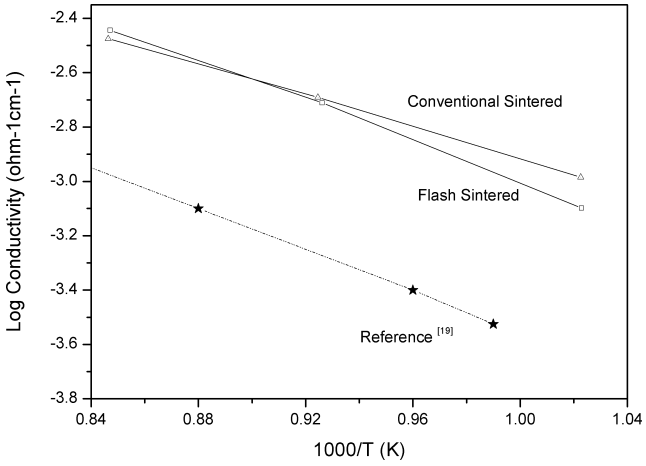

Fig. 12. Arrhenius plot of the conductivity of flash sintered (□) and conventional sintered $SrTiO_3$ (Δ). Reference (dash line-star) is given for comparison.[19]

caused by differences in stoichiometry. It is known that the conductivity of $SrTiO_3$ can change easily with even small compositional changes such as oxygen deficiency, slight change in the Sr/Ti ratio or formation of Ruddlesden–Popper phases.[20–25] Together, the optical spectroscopy, XRD, PIXE, conductivity measurements, and TEM revealed that sintering, either conventionally or flash, results in non-stoichiometric phases. The defect states detected by optical spectroscopy and by the peak shift in the XRD are due to distortions in the cubic structure as a consequence of the formation of RP phases.

In a previous work, we reported that undoped Al_2O_3 did not show any flash sintering phenomenon[5]; flash sintering could only be achieved upon doping with MgO. In the case of flash-sintered SrTiO3, we believe that non-stoichiometry in the form of RP phases, enhances the sintering process *via* an enhancement of conductivity which is particularly important for the flash sintering process. Clearly, the defect structure of the material is important for the propensity for flash sintering to occur. Although the flash sintered and conventional sintered samples have some qualitative similarities, the flash-sintered material has an overall lower defect content, as determined by optical analysis and XRD. Thus, the differences are in number rather than kind.

IV. Conclusion

Strontium titanium oxide is flash sintered at different applied fields to understand the role of the field strength on density and grain growth. The density increased with decreasing applied voltages, which is in contrast with the trend observed in ionically or electronically conductive ceramics (YSZ, Co_2MnO_4, etc.). The highest density material (more than 95%) is obtained for fields of 150 V/cm. At this applied voltage, flash sintering occurred at 1200°C. The density of conventionally sintered $SrTiO_3$ at 1400°C is 5% lower than that in this sample. Grain growth followed a similar trend as density and abnormal grain growth, observed in conventional sintered sample, is arrested by flash sintering.

Optical and structural characterization reveals that sintering, either conventional or flash, induced the formation of non-stoichiometric phases in $SrTiO_3$. We believe that these defects assisted the occurrence of flash sintering in pure $SrTiO_3$ as flash sintering did not occur in undoped Al_2O_3. Indeed, flash sintering was only achieved in Al_2O_3 upon doping with MgO. It is suggested that the non-stoichiometric RP phases play an important role in the processes associated with the flash sintering of $SrTiO_3$.

Acknowledgments

This project is supported by Center for Materials at Irradiation and Mechanical Extremes (CMIME), an Energy Frontier Research Center funded by the U.S. Department of Energy, Office of Science, Office of Basic Energy Sciences under Award Number 2008LANL1026; Mike Nastasi, PI and by the Basic Energy Sciences Division of the Department of Energy under Grant no.: DE-FG02-07ER46403. Authors would like to thank to Yongqiang Wang (IBML-LANL) for PIXE measurements. We are also grateful to Darrick Williams and Mujin Zhuo(CINT-LANL); and Kurt Sickafus, James Valdez, Maulik Patel and Ellen Cerreta (MST-8, LANL) for their efforts and time.

References

[1]M. Cologna, A. L. G. Prette, and R. Raj, "Flash-Sintering of Cubic Yttria-Stabilized Zirconia at 750°C for Possible Use in SOFC Manufacturing," *J. Am. Ceram. Soc.*, **94**, 316–9 (2011).

[2]Z. A. Munir, U. Anselmi-Tamburini, and M. Ohyanagi, "The Effect of Electric Field and Pressure on the Synthesis and Consolidation of Materials: A Review of the Spark Plasma Sintering Method," *J. Mater. Sci.*, **41**, 763–77 (2006).

[3]M. Cologna, B. Rashkova, and R. Raj, "Flash Sintering of Nanograin Zirconia in o5 s at 850°C," *J. Am. Ceram. Soc.*, **93**, 3556–9 (2010).

[4]A. L. G. Prette, M. Cologna, V. Sglavo, and R. Raj, "Flash-Sintering of Co_2MnO_4 Spinel for Solid Oxide Fuel Cell Applications," *J. Power Sources*, **196**, 2061–5 (2011).

[5]M. Cologna, J. S. C. Francis, and R. Raj, "Field Assisted and Flash Sintering of Alumina and its Relationship to Conductivity and MgO-Doping," *J. Eur. Ceram. Soc.*, **31**, 2827–37 (2011).

[6]M. Cologna and R. Raj, "Surface Diffusion-Controlled Neck Growth Kinetics in Early Stage Sintering of Zirconia, with and without Applied DC Electrical Field," *J. Am. Ceram. Soc.*, **94**, 391–5 (2011).

[7]M. Cologna, M. Bertoldi, and V. M. Sglavo, "Sintering and Deformation of Solid Oxide Fuel Cells Produced by Sequential Tape Casting," *Int. J. Appl. Ceram. Technol.*, **7**, 803–13 (2010).

[8]E. C. M. Pennings and W. Grellner, "Precise Nondestructive Determination of the Density of Porous Ceramics," *J. Am. Ceram. Soc.*, **72**, 1268–70 (1989).

[9]Joint Committee on Powder Diffraction Standards Card No. 73-0661, International Center for Diffraction Data, Newton Square, PA, 2005.

[10]S. N. Ruddlesden and P. Popper, "The Compound SrsTi207 and its Structure," *Acta Cryst.*, **11**, 54–5 (1958).

[11]D. C. Meyer, A. A. Levin, T. Leisegang, E. Gutmann, P. Paufler, M. Reibold, and W. Pompe, "Reversibletuning of a Series of Intergrowth Phases of the Ruddlesden–Popper Type $SrO(SrTiO_3)_n$ in an (001) $SrTiO_3$ Single-Crystalline Plate by an External Electric Field and its Potential Use for Adaptive X-Ray Optics," *Appl. Phys. A*, **84**, 31–5 (2006).

[12]R. J. D. Tilley, "An Electron Microscope Study of Perovskite-Related Oxides in the Sr-Ti-O System," *J. Solid State Chem.*, **21**, 293 (1977).

[13]D. Fuchs, M. Adam, P. Schweiss, S. Gerhold, S. Schuppler, R. Schneider, and B. Obst, "Structural Properties of Slightly off-Stoichiometric Homoepitaxial $SrTi_xO_{3-\delta}$ Thin Films," *J.Appl. Phys.*, **88**, 1844 (2000).

[14]D. C. Meyer, A. A. Levin, S. Bayer, A. Gorbunov, W. Pompe, and P. Paufler, "An Electrical Field-Induced Structural Effect in Strontium Titanate at Room Temperature," *Appl. Phys. A*, **80**, 515–22 (2005).

[15]W. Tian, J. H. Haeni, D. G. Schlom, E. Hutchinson, B. L. Sheu, M. M. Rosario, P. Schiffer, Y. Liu, M. A. Zurbuchen, and X. Q. Pan, "Epitaxial Growth and Magnetic Properties of the First Five Members of the Layered $Sr_{n+1}Ru_nO_{3n+1}$ Oxide Series," *Appl. Phys. Lett.*, **90**, 022507 (2007).

[16]D. Music and J. M. Schneider, "Elastic Properties of $Sr_{n+1}Ti_nO_{3n+1}$ Phases (n = 1–3, ∞)," *J. Phys. Condens. Matter*, **20**, 055224 (2008).

[17]J. H. Haeni, C. D. Theis, D. G. Schlom, W. Tian, X. Q. Pan, H. Chang, I. Takeuchi, and X.-D. Xiang, "Epitaxial Growth of the First Five Members of the $Sr_{n+1}Ti_nO_{3n+1}$ Ruddlesden–Popper Homologous Series," *Appl. Phys. Lett.*, **78**, 3292 (2001).

[18]W. Tian, X. Q. Pan, J. H. Haeni, and D. G. Schlom, "Transmission Electron Microscopy Study of n = 1–5 $Sr_{n+1}Ti_nO_{3n+1}$ Epitaxial Thin Films," *J. Mater. Res.*, **16**, 2013–26 (2001).

[19]N. H. Chan, R. K. Sharma, and D. M. Smith, "Nonstoichiometry in $SrTiO_3$," *J. Electrochem. Soc.*, **128**, 1762 (1981).

[20]A. Kalabukhov, R. Gunnarsson, J. Börjesson, E. Olsson, T. Claeson, and D. Winkler, "Effect of Oxygen Vacancies in the $SrTiO_3$ Substrate on the Electrical Properties of the $LaAlO_3/SrTiO_3$ Interface," *Phys. Rev. B*, **75**, 121404(R) (2007).

[21]J. Gerblinger and H. Meixner, "Electrical Conductivity of Sputtered Films of Strontium Titanate," *J. Appl. Phys.*, **67**, 7453 (1990).

[22]H. Hayashi, H. Inaba, M. Matsuyama, N. G. Lan, M. Dokiya, and H. Tagawa, "Structural Consideration on the Ionic Conductivity of Perovskite-Type Oxides," *Solid State Ionics*, **122**, 1 (1999).

[23]W. Menesklou, H.-J. Schreiner, K. H. Hardtl, and E. Ivers-Tiffee, "High Temperature Oxygen Sensors Based on Doped $SrTiO_3$," *Sensors Actuat. B*, **59**, 184–9 (1999).

[24]K. Morito, T. Suzuki, and M. Fujimoto, "Microstructure and Electrical Properties of Nonstoichiometric Strontium Titanate Thin Films Grown on Platinum Electrodes," *Jpn. J. Appl. Phys.*, **40**, 1310–4 (2001).

[25]J. W. Fergus, "Perovskite Oxides for Semiconductor-Based Gas Sensors," *Sensors Actuat. B*, **123**, 1169–79 (2007). □